

A passive metallic damper with replaceable steel bar components for earthquake protection of structures

Reza Aghlara^a, Mahmood Md. Tahir^{b,*}

^a Faculty of Civil Engineering, Universiti Teknologi Malaysia, 81310 Johor Bahru, Johor, Malaysia

^b Institute for Smart Infrastructure & Innovative Construction (ISIIC), Faculty of Civil Engineering, Universiti Teknologi Malaysia, 81310 Johor Bahru, Johor, Malaysia

A B S T R A C T

In this paper, a new passive earthquake damper termed as Bar-Fuse Damper (BFD) is presented for frame structures. The BFD is developed from common steel sections such as hot-rolled Square Hollow Sections (SHS), C-channels, plates and bars. It is economical, easy to install and build with no special fabrication technique. The key feature of the BFD is using round steel bars as energy absorber components that can be easily replaced in case of failure. The proposed device dissipates the energy with the replaceable bars as sacrificial elements through the flexural and tensile mechanism. The performance of several full-scale BFDs was evaluated with a series of monotonic and cyclic experiments, and the bars successfully performed their function as energy absorbers and fuses in all specimens. The effects of variations in the number, length and diameter of bars in the BFD along with the nuts arrangement were investigated in this experimental study. This study indicates that the recommended device has stable hysteretic behaviour under cyclic loads with two significant features: appropriate energy dissipation and replaceability of the fuses, which can be useful to protect the main elements of structures from plastic deformation and failure for several events. The results obtained for the BFD are promising for its use as a passive seismic damper in engineering structures in order to improve the seismic behaviour of structures as well as dissipating the earthquake energy.

1. Introduction

Generally speaking, structural control can be categorized as active, semi-active and passive control [1]. In active and semi-active control systems, the structural response varies based on the characteristics of the forces applied to the structure by an earthquake or wind. In other words, the structural response to the applied forces is adjusted by a control system to sustain the input loads. These control systems may consist of a power supply, sensors and hydraulic jacks [2]. On the other hand, the passive structural control is independent of the forces applied by an earthquake or wind and only depends on the type of equipment and material that were used in the damper. The main goal of the passive control systems is to reduce the contribution of the principal structural elements in dissipating the input energy by plastic deformation. Base isolators, metallic yielding dampers, friction dampers, viscous and viscoelastic dampers, tuned mass and liquid dampers are all classified as passive control systems [3,4].

In spite of their simplicity, metallic yielding dampers, as structural control systems, offer special features such as economic efficiency, while requiring neither advanced technology nor experts for fabrication

and installation of the system. Another advantage of such dampers is the simplicity of their simulation through mathematical and finite element models, which is helpful in designing and predicting their behaviour. The energy dissipation in this type of damper is carried out by plastic deformation in different mechanisms such as bending, shear, torsion or a combination of them in the energy absorbers. Metallic dampers were first manufactured in Japan and New Zealand about 50 years ago. In Japan, Muto and Guerrero have implemented slitted wall and damping strips for partition walls respectively, in a number of buildings for earthquake energy dissipation [5,6]. In New Zealand, Kelly and Skinner have carried out experimental investigations on energy absorbers such as torsional beams, u-strips and flexural beams [7,8].

ADAS (Added Damping and Stiffness) and SSD (Steel Slitted Damper) are among the most familiar metallic yielding dampers that have been put into use in buildings in the US, Japan, Italy and Mexico [3,9]. ADAS consists of a series of X- or triangular-shaped steel sheets that dissipate the energy applied to the structure by bending [10]. The SSD damper is composed of one or more slitted sheets that dissipate energy through planar deformation and shear-bending mechanisms

* Corresponding author.

E-mail addresses: areza24@live.utm.my (R. Aghlara), mahmoodtahir@utm.my (M.Md. Tahir).

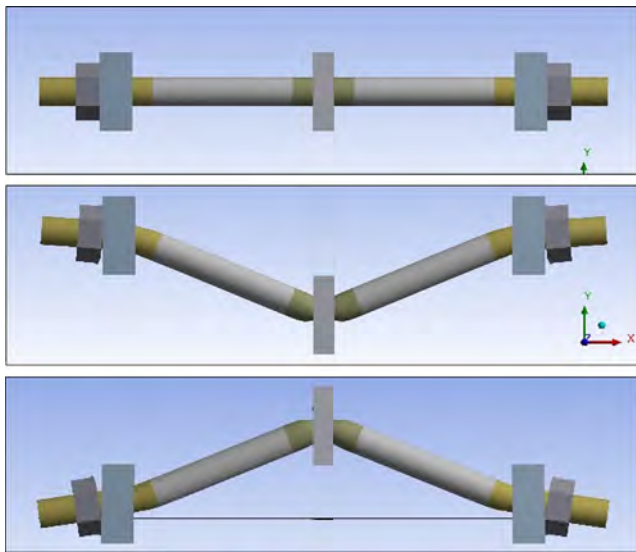


Fig. 1. Deformed and un-deformed states of a bar.

[11]. The two dampers named here are particular to Chevron braced frames and cannot be implemented on diagonal-braced frames. A new type of metallic damper, known as CSYB (Cast-Steel Yielding Brace), was introduced in Canada which is very similar to TADAS in performance [12]. Only different in that it is made of cast steel instead of steel and can be implemented in diagonal braced frames. Researchers have extensively studied new metallic dampers in recent years [13–16]. Some researchers, interestingly, gave the name fuse to metallic dampers, given that they are sacrificed in keeping the principal elements of

the structure safe from damage [12,17,18]. Although, many of these dampers do not seem to be easy to replace after failure.

Generally, the two important characteristics attributed to fuses are that they are made of inexpensive materials and are easily replaced. Considering these features, a new metallic yielding damper, named Fuse Damper (FD), was designed so that the replaceable parts, or fuses, offer reasonable energy dissipation by bending, as shown in Fig. 1. The fuses used in this damper can be made of any material, and in any cross-section geometry, provided that they have adequate energy absorption characteristics. Six factors control the behaviour of this damper, namely: the material and shape of the parts, the number of the parts, the dimensions (length and width) of the parts, and the fixing method of the parts. The body and geometry of the damper are rigidly designed to transfer all the displacement of the device to the fuses, thus being plastically deformed. In the first stage, a round steel bar was used as the fuse or sacrificial element, and the setting was named Bar-Fuse Damper (BFD). Provided it fulfils the requirements of a metallic damper, significant advantages can be cited for this device, including: the low weight of the fuses, their low cost, ease of replacement, fabrication with no need for complex and expensive material and equipment, the possibility of the device being made on the construction site, no need for maintenance during operation, applicable to different frame configurations, and familiarity of operation engineers with the material used and its behaviour. It should be noted that, as an advantage, the suggested damper only acts under earthquake force and has no role in resisting the static loads of the structure.

The aim of this study is to evaluate the characteristics of the BFD individually. The outline of this study can be summarized as follows: after initially designing the BFD, the effect of the rebar nuts configuration on the behaviour of the dampers was evaluated through a number of experiments and the most efficient configuration was

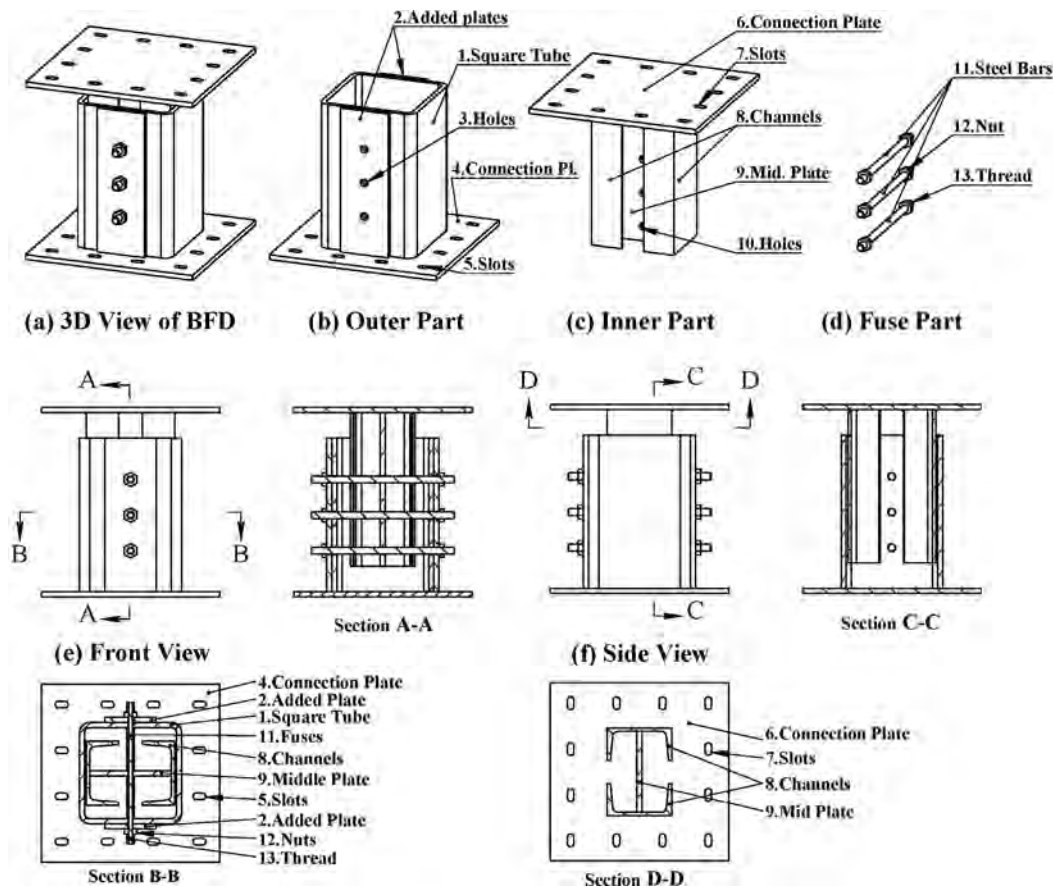


Fig. 2. Geometric illustration of the Bar-Fuse Damper (BFD).

selected. Then, in order to evaluate the hysteretic behaviour of the BFD, a series of quasi-static cyclic tests were performed, calculating the important mechanical characteristics of the BFD based on test results. Moreover, a parametric study was performed based on the experimental data and a series of formulas were presented for the mechanical characteristics, together with a design chart that can be used in the initial design process of the BFD. Then a two-line model equivalent to spring behaviour was computed and presented for the analysis software. Furthermore, the BFD was modelled by ANSYS to compare the results of non-linear analysis and the experiments. Finally, a comparison was made between well-known metallic dampers and the BFD based on their mechanical features. The main findings of this study are presented in the final section of this paper, which suggests the possibility of implementing BFD as metallic dampers in structures.

2. Bar-Fuse Damper

The basic geometry of the proposed device is illustrated in Fig. 2. The Bar-Fuse Damper (BFD) (a) comprise three main parts; an outer part (b), an inner part (c) and a fuse part (d). The outer and inner parts are rigid and are connected to each other by the flexible fuse part. The outer part is fabricated as a square tube with some facing holes in its web, a connection plate with some slots to attach the part to the brace member, and two perforated flat plates welded to the square tube to prevent its body from crippling, and to make safe supports for the fuses. The inner part is made up of two structural channel sections welded to each other symmetrically by a perforated flat plate. All the described components of the outer part and the inner part are welded properly together to make rigid parts. The fuse part includes replaceable steel bars with both ends threaded, as the yielding components of the damper which can be readily installed in the device by nut fasteners. The bending length, diameter and quantity of the bars can control the mechanical characteristics of the BFD, such as strength and stiffness. Due to the axial tension/compression force of the brace members, the inner part moves back and forth inside the outer part and causes deformation in the bars.

The Bar-Fuse Damper (BFD) dissipates energy based on plastic deformation of the steel bar. In this damper, the mechanism of energy dissipation depends directly on the range of bar deformation. The flexural mechanism plays a main role in energy dissipation at small displacements, while it transforms to the tensile mechanism at relatively large displacements. The mentioned transformation of the dissipation mechanism from flexural to tensile increases the secondary stiffness and strength of the BFD to a much higher value.

Fig. 3 shows three suitable configurations in which the Bar-Fuse Damper was added to the frame of a structure. The BFD for the middle of the braces can be set up in diagonal and chevron braces as shown in Fig. 3(a) and (b). As an advantage compared to other metallic dampers, there are fewer limitations to install the BFD in a frame. For instance, it can be applied as a connection of the brace to the frame, as shown in Fig. 3(c), although, some modifications in the geometry of the parts are necessary. In this case, the gusset plates of the braces connection perform the same function as the inner part of the BFD. However, it might be subjected to unexpected forces as moments due to rotations, which should be considered in design and construction of the proposed device.

3. Experimental study

The purpose of the experiments is to verify the structural characteristics and efficiency of the BFD. Monotonic and quasi-static cyclic loading tests were performed on several specimens to evaluate the energy dissipation capacity, along with the cyclic performance and behaviour of the BFDs. The diameter, length and number of the steel bars, as three key parameters of the BFD, were studied in this experimental verification. Similarly, a series of experiments were conducted on the device to study the influence of different nut configurations on

the performance of the BFDs. To obtain the ultimate strength and displacement of the steel bars, monotonic tests were conducted for some specimens until failure of the bars. These results were also helpful for evaluating the yielding load and yielding displacement of the BFDs.

3.1. Specimens

A total of three specimens were fabricated at the structural lab of University Teknologi Malaysia (UTM). To make the specimens reusable for several experimental tests, the outer and inner parts of the BFDs were designed to be rigid, so that the bars would carry all the applied loads through bending. Therefore, these parts were used for several tests to study the influence of different diameters, quantities and bending length of the steel bars on the behaviour of the BFD. To assess the effect of different bending lengths of the bars, the inner distance of the tubes was reduced by welding two perforated flat plates inside the square tubes of the BFDs properly. Table 1 lists the dimensions of the applied components which were used for fabrication of the main parts.

To acquire the mechanical properties of the bars, 13 tension coupon tests (at least three tests for each diameter of bars) were completed on specimens of bars, following the ASTM A370 standard [19]. The average values for the mechanical properties of bars are calculated and listed in Table 2.

To simplify the naming of specimens in tests, a particular configuration has been defined for their names in the general form [No. 1] [ELEMENT][No. 2]-[No. 3]. No. 1 indicates the number of fuses in the BFD, which it is the number of bars. The second term, ELEMENT, shows the type of fuse component, such as a bar. No. 2 shows the diameter of the applied fuse, and No. 3 stands for the bending length of the fuse. As mentioned earlier, the fuse element is a round steel bar in this paper, which is normally used in the concrete structures. The list of monotonic and cyclic tests with relevant information about specimens is tabulated in Table 3.

3.2. Tests setup and loading protocol

An INSTRON8801 testing machine was used in the UTM structural lab, to investigate the performance of the BFDs. Fig. 4 shows the test setup of this experimental study. Two particular controller software, BlueHill and WaveMaker, were used for the monotonic and quasi-static cyclic tests respectively. This testing machine can report the displacements and load history directly to a computer in real-time.

Two rigid transition parts, as shown in Fig. 4, were fabricated from structural steel, to make the installation of BFDs on the testing machine feasible. The transition part comprised an inner threaded tube with a flange at one end (for connecting to the testing machine), and a thick slotted plate at the other end (for connecting to the inner or outer parts of the BFDs through M12 bolts). The function of the transition part was to transfer uniformly the axial load from the actuator to the specimen, as well as providing a suitable platform to mount easily the BFD on the testing machine. Considering that the metallic dampers are relatively independent of the rate of the loading, the loading speed was selected in the range of 5–20 mm/min, depending on displacement amplitude in the loading protocol. Fig. 5 shows the testing apparatus and the specimen of 3BFD10-188 before the cyclic test.

The Quasi-Static Cyclic tests were carried out on the BFDs under displacement control within the elastic and inelastic range. The displacement history was calculated according to FEMA461 protocol 1 [20]. The required maximum displacements (Δ_m) for calculating the displacement amplitudes of loading histories were determined based on ultimate displacements obtained from the monotonic tests. The displacement amplitudes for different load protocols were calculated for each step based on the protocol procedure, as listed in Table 4.

According to the FEMA461, two cycles with equal displacement were allocated to each step of the loading history. If the specimen had not failed at the estimated maximum displacement (Δ_m), the test was

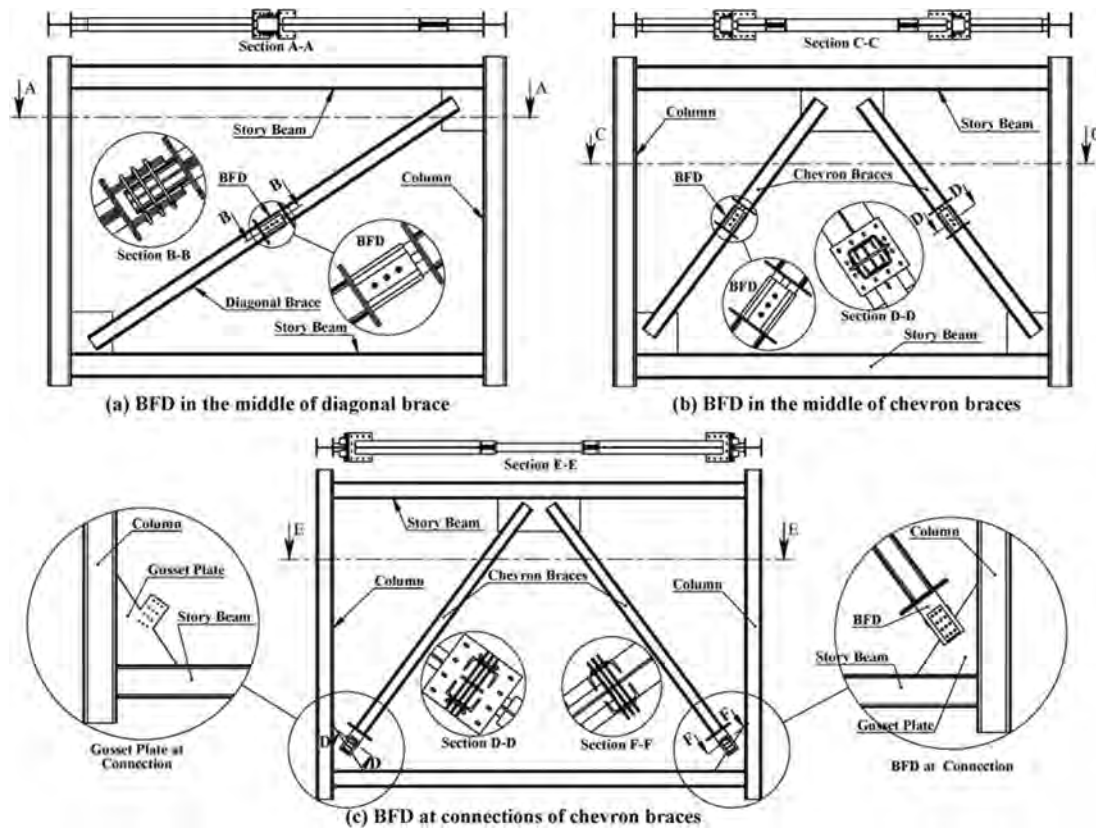


Fig. 3. Possible configurations for installation of the BFD in a frame.

Table 1
Components dimension of the BFD.

Parts	ID	Components	QTY	Length (mm)	Width (mm)	Depth (mm)	Flange width (mm)	Thickness (mm)	Diameter (mm)	Description
Outer part	1	Square tube (BSI)	1	300	200	200	–	6	–	6 Holes 11/13/15 mm
	2	Added plate (outside)	2	300	100	–	–	10	–	3 Holes 11/13/15 mm
	4	Connection plate	1	350	350	–	–	10	–	12 Slots for M12
	–	Added plate (inside)	2	300	60	–	–	15	–	3 Holes 11/13/15 mm
Inner part	6	Connection plate	1	350	350	–	–	10	–	12 Slots for M12
	8	RSC Channels (BSI)	2	300	–	127	64	6.4	–	–
	9	Middle plate	1	300	160	–	–	10	–	3 Holes 11/13/15 mm
Fuse part	11	Round bar	–	280	–	–	–	–	10, 12, 14	35 mm Threaded Ends

Table 2
Material properties of steel bars.

Bar diameter (mm)	Modulus of elasticity (GPa)	Yield stress (MPa)	Ultimate stress (MPa)	Elongation (%)
10	228	450	468	13
12	216	569	601	18
14	210	517	554	14

followed by increased amplitudes of $(1.3\Delta_m)$ for every single cycle until complete failure.

3.3. Selection of proper nuts configuration

As mentioned earlier, the performance of the BFD highly depends on the nuts configuration of the applied bars. In fact, the nuts configuration has a major role on changing the bars reaction to the applied loads. In other words, this feature can alter the energy-dissipating mechanism in the BFD. To study and verify the influence of various nuts

configurations, a total of three experiments were performed on the BFD with the INSTRON testing machine. Three nuts configurations, Type A, B and C as shown in Fig. 6(a)/(b)/(c), were tested for the proposed device. Type A is a normal configuration (NC) including nuts at both ends of the threaded bar, as shown Fig. 6(d), on the outside of the outer part. This is the simplest configuration for mounting and replacing the bars in the BFDs. In Type B and C, as shown in Fig. 6(e) and (f), a Fully Threaded Bar (FTB) was used with two more nuts inside the outer part, as Nuts on Both Sides (NBS) or Nuts in the Middle (NIM), as also shown in Fig. 6(e) and (f) respectively. In addition, to study the influence of different materials of the bar in the BFD, one high strength FTB was evaluated with the Type A nut configuration, as shown in Fig. 6(g).

The output of the above experimental studies is the force-displacement hysteresis, as shown in Fig. 7(a) and (b), which is useful to assess the effect of different nuts configurations on the behaviour of BFDs. The shape of the curves for specimen 1FTB10-188 with Type B nut configuration is not very stable at the unloading segment and at loading in the reverse segment (minus sign). Type C shows more stable behaviour than Type B, but it bears a lower number of loading cycles compared

Table 3
List of specimens and experiments.

Specimens	Bars			Tests	
	Diameter (mm)	Length ^a (mm)	QTY	Monotonic	Cyclic
1Bar10-188	10	188	1	×	×
2Bar10-188	10	188	2	×	×
3Bar10-188	10	188	3	×	×
1Bar10-158	10	158	1	×	×
2Bar10-158	10	158	2	×	×
3Bar10-158	10	158	3		×
1Bar12-188	12	188	1	×	×
2Bar12-188	12	188	2	×	×
3Bar12-188	12	188	3	×	×
1Bar12-158	12	158	1	×	×
2Bar12-158	12	158	2		×
3Bar12-158	12	158	3		×
1Bar14-188	14	188	1	×	×
2Bar14-188	14	188	2	×	×
3Bar14-188	14	188	3	×	×
1Bar14-158	14	158	1	×	×
2Bar14-158	14	158	2		×
3Bar14-158	14	158	3		×

^a Bending length of the bars (free inside distance of Square Tube).

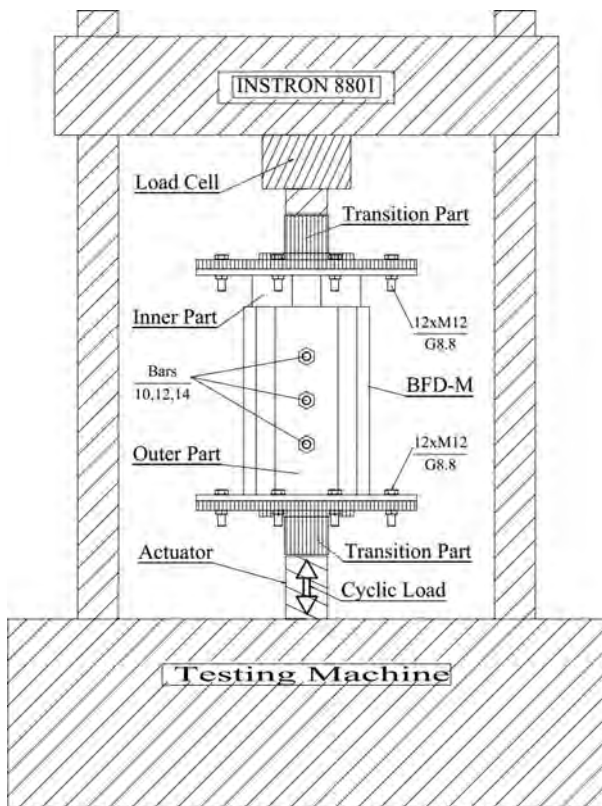


Fig. 4. Setup of experimental tests.

with Type A. As expected, the high strength bar – 1FTB10-188 (HS)(NC) – exhibited stable cycles with more stiffness and strength relative to the others, but without desired ductility, which makes it inappropriate for a metallic damper. Specimen 1Bar10-188 with Type A nuts configuration shows a stable force-displacement relationship during the test along with bearing more loading cycles compared to the rest. In addition, another benefit of Type A is its simplicity in placing and replacing the bars in the BFD. Consequently, Type A was selected for the BFD as the best nuts configuration for the subsequent experimental studies.



Fig. 5. Testing apparatus.

Table 4
Calculated displacements for different load protocols (in mm).

Steps	Cycles	Load protocols		
		LP 20	LP 30.4	LP 36.7
1	1, 2	0.96	1.46	1.78
2	3, 4	1.35	2.04	2.49
3	5, 6	1.89	2.86	3.48
4	7, 8	2.64	4.00	4.87
5	9, 10	3.70	5.61	6.82
6	11, 12	5.18	7.85	9.55
7	13, 14	7.25	10.99	13.37
8	15, 16	10.15	15.38	18.72
9	17, 18	14.21	21.53	26.21
10	19, 20	20.00	30.40	36.69
11	21	26.00	39.1	45
12	22	33.80	50.1	58.5

3.4. Experimental results and discussions

3.4.1. Monotonic tests

A series of monotonic tests were conducted on the BFDs to obtain the key parameters of the mechanical characteristics. Fig. 8(a) shows the test setup for the monotonic experiments. The force was applied to the outer part of the specimens in a downward direction at a constant rate until complete failure. The speed of loading was adjusted in the range of 5–10 mm/min for all the tests. The failure modes of some bars are also shown in Fig. 8(b–d).

Fig. 9 shows the force-displacement curves of the BFDs obtained from the above mentioned monotonic tests. The yield points of specimens are not distinctly observable and all of them are relatively small amounts less than 3.20 mm. The shapes of the curves in this figure show that the behaviour of the bars is completely different from the bilinear behaviour of pure bending, and there is a considerable growth in strength after yielding. This indicates that the dissipation mechanism in this device is a flexural-tensile mechanism. As can be seen in the figure, with a constant bar length, increasing the bar diameter gives rise to four important parameters of the device: elastic stiffness (K_0), secondary stiffness (K_p), strength (P_u) and ultimate displacement (D_u). On the other hand, increasing the bar length with a constant diameter generally cause the ultimate displacement of the BFD to increase noticeably

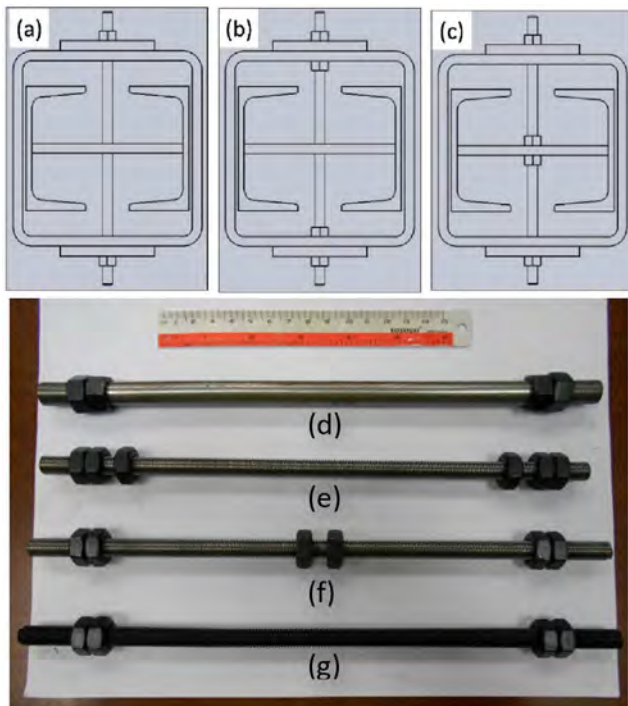


Fig. 6. Nuts configurations (a) Type A (NC), (b) Type B (NBS), (c) Type C (NIM), (d) Both ends of the threaded bar (NC) (e) FTB (NBS), (f) FTB (NIM), (g) High strength FTB (NC).

along with decreases in the strength, elastic stiffness, and secondary stiffness of the device.

Table 5 highlights the key values obtained from monotonic tests for the BFDs. The ratio of ultimate displacement to yielding displacement, ductility (μ), and the ratio of ultimate displacement to the bending length, deformation capacity (D_{cap}), were also calculated and tabulated in Table 5. As can be seen from this table, the yielding displacement (D_y) is a quite small amount less than 3.20 mm. This amount includes the clearance gap between the bar and the related hole of the inner part, which is provided for easy installation of the bars. The average ductility (μ) and deformation capacity (D_{cap}) of the BFD are 13.85 and 19%, respectively. It is believed that these values can be improved by using milder material for the bars of the device. Regarding the increasing trend of the strength, although this hardening response is alleviated under cyclic loads, it should be taken into account in the design of connecting members to the BFD. In other words, the ultimate strength of connected elements to the BFD such as braces and connections should be taken greater than the maximum strength of the proposed device.

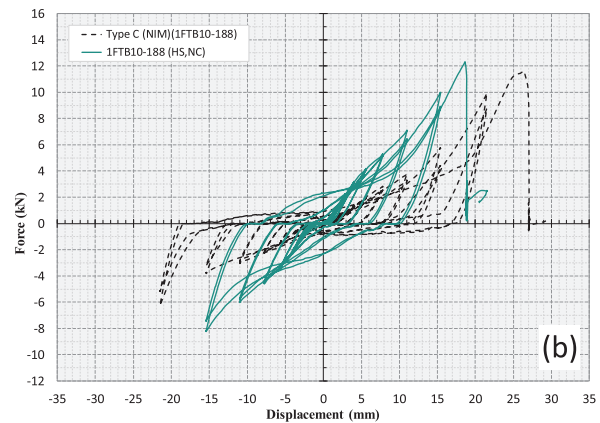
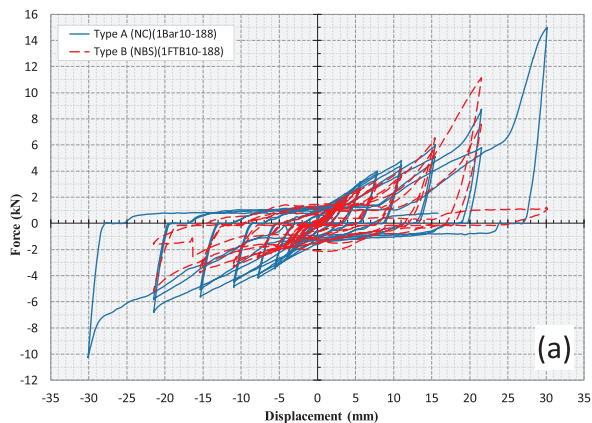


Fig. 7. Force-displacement hysteresis for different nuts configurations of the BFD; (a) Type A, -B, (b) Type C, 1FTB10-188.

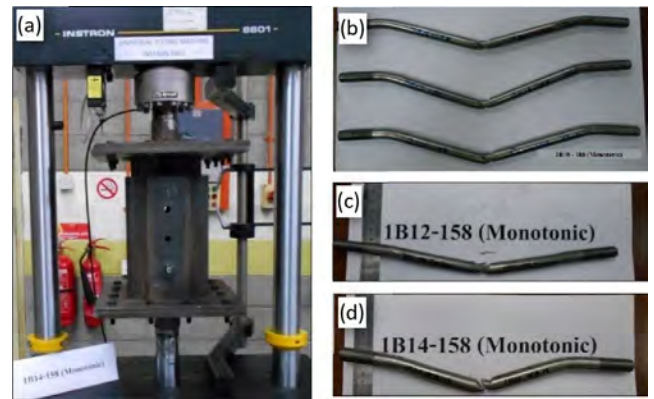


Fig. 8. Setup of the monotonic tests and the failure modes; (a) 1Bar14-158, (b) 3Bar10-188, (c) 1Bar12-168, (d) 1Bar14-158.

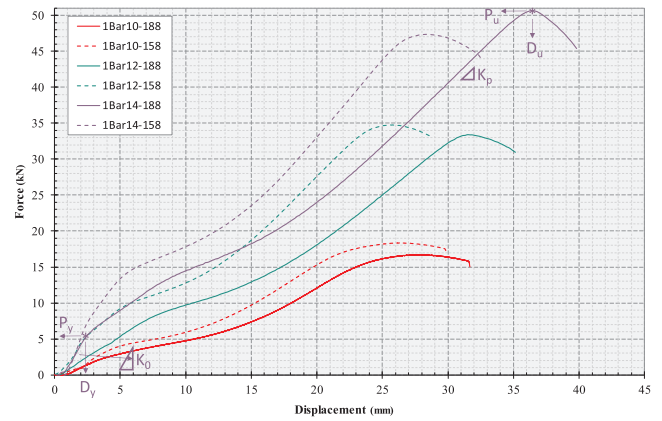


Fig. 9. Experimental force-displacement relation of monotonic tests.

Table 5
Important values from the monotonic tests.

Specimens	D_y (mm)	P_y (N)	K_0 (N/mm)	P_u (kN)	D_u (mm)	μ (D_u/D_y)	D_{cap} (D_u/L)
1Bar10-188	3.00	1350	450.0	16.72	31.67	10.6	0.17
1Bar10-158	1.90	1810	952.6	18.32	29.85	15.7	0.19
1Bar12-188	3.17	3095	976.3	33.38	35.17	11.1	0.19
1Bar12-158	2.08	4560	2192.3	34.78	28.25	13.6	0.18
1Bar14-188	2.33	5140	2206.0	50.61	39.83	17.1	0.21
1Bar14-158	2.16	5880	2722.2	47.34	32.50	15.0	0.21

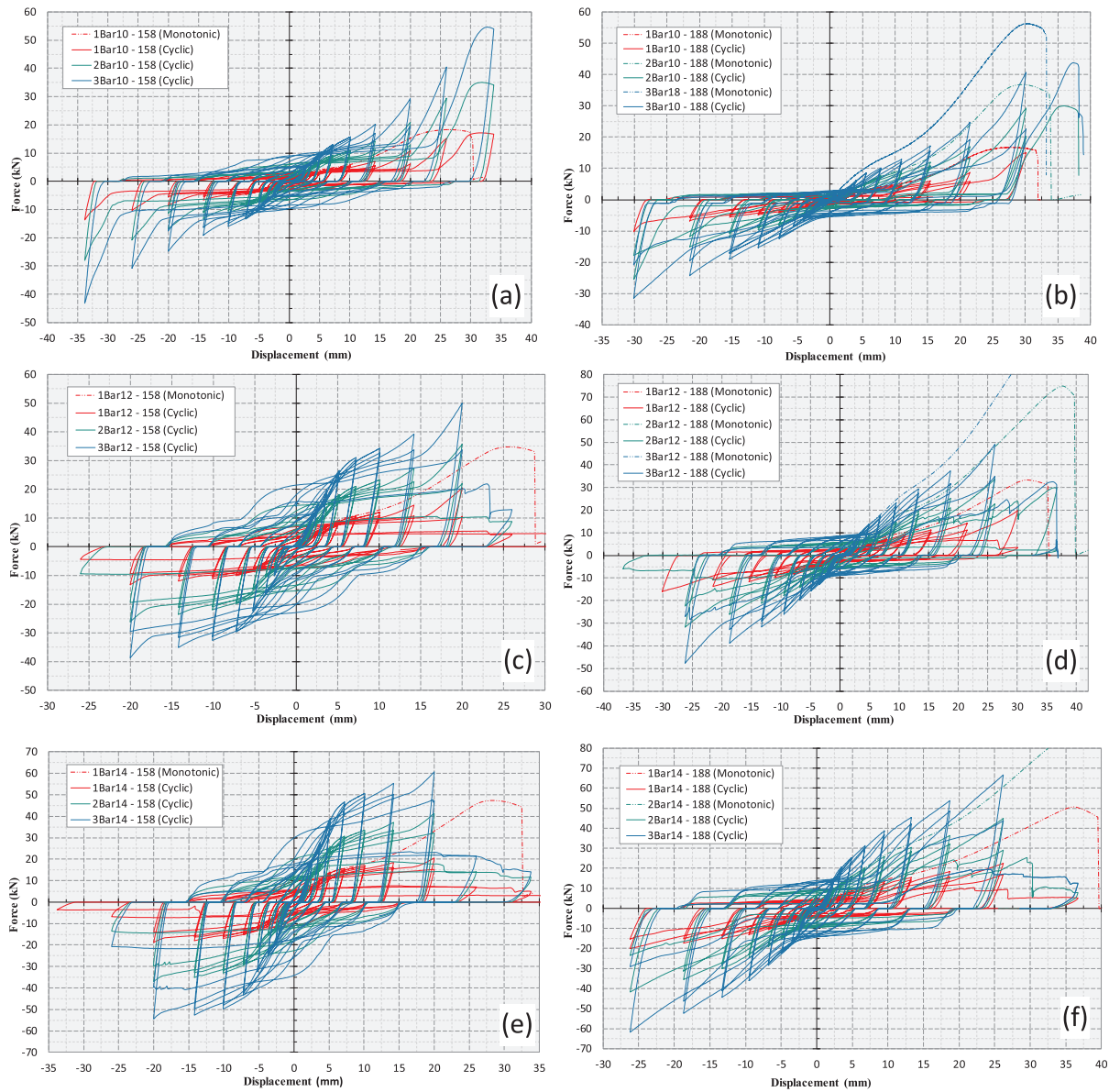


Fig. 10. Experimental cyclic force-displacement hysteresis of specimens with different number, diameter and length of bars; (a) 1/2/3BFD10-158, (b) 1/2/3BFD10-188, (c) 1/2/3BFD12-158, (d) 1/2/3BFD12-188, (e) 1/2/3BFD14-158, (f) 1/2/3BFD14-188.

3.4.2. Cyclic tests

A total of 18 specimens with different key geometric parameters such as the bar number, length and diameter were experimentally tested under quasi-static cyclic loading regimes. The objective of the experiments was to study the performance of BFDs in several aspects, as well as an assessment of the structural characteristics, and to evaluate the effect of various key factors on the behaviour of the proposed device. Three devices (BFD10, BFD12 and BFD14) were fabricated for three different bar diameters, 10, 12 and 14 mm. Each device was used a total of 6 times for the cyclic experiments, each time with three different numbers of the bars (1, 2 and 3 bars) and two different lengths of bars (158 and 188 mm). All the specimens were loaded by displacement control at a rate of 10 mm/min until failure, according to the FEMA461 load protocol which was presented before in Table 4. Two cycles were completed for each amplitude of the loading history. The tests were performed until complete failure of the specimens and the exact location of all the fractures was at the middle of the bars in the tests.

Fig. 10 shows the force-displacement hysteresis of 18 specimens which were experimentally obtained under the quasi-static cyclic tests. A positive sign refers to the downward displacement imposed on the

outer part of the specimen. All the bars deformed in a stable and similar manner. Like the monotonic tests results, the yielding points occurred at small displacements and there was a smooth transition between elastic and inelastic behaviour. All the BFDs showed appropriate ductility, energy absorption and stable hysteresis loops with no sudden strength and stiffness degradation in the system. In all of the hysteresis curves, the strength and stiffness of BFDs increase when applying a greater number of bars, as expected. Similar to the results of the monotonic tests, the strength increases proportionally with the adding of the bars, for the same bar length and diameter. For constant bar length, increase of the bar diameter leads to the growth of strength and stiffness while the increase of the bar length for a constant diameter causes a reduction of strength and stiffness.

As can be seen in Fig. 10, the considerable pinching is observable in hysteresis loops of all the specimens. Pinching is a recognised phenomenon in some seismic resisting systems and damping systems, such as concrete shear walls and shape memory alloy dampers. In unloading phase of the BFD's response, the flexural mechanism individually contributed in resisting force, and since its amount is less than resisting force when the mechanism is flexural-tensile, the decrease in both

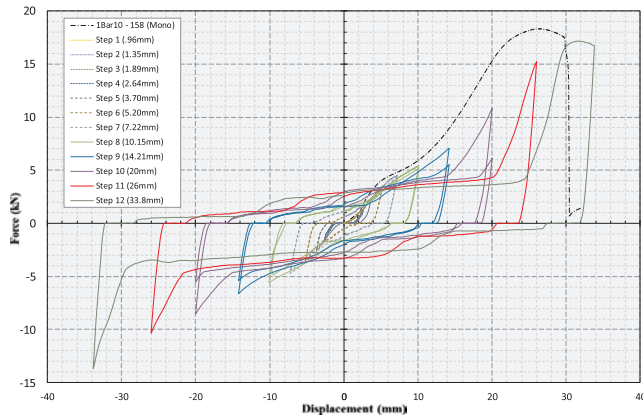


Fig. 11. Force-displacement hysteresis of specimen 1Bar10-158.

strength and stiffness – pinching – occurs in this part of response. having a small contribution of the BFD in lateral-resisting system, the pinching cannot be pronounced as a deleterious effect on response of global system, and it only causes reduction in energy dissipation capacity of the proposed device. As an advantage, a system with pinching can sway conveniently back to its origin at the end of vibration without any resisting force induced by elements of damping system. Accordingly, it decreases both residual force and displacement in members of structure at the end of excitation.

To have a detailed evaluation of the BFD performance, the force-displacement hysteresis of one specimen 1Bar10-158 is illustrated in Fig. 11. Comparing the results obtained from monotonic and cyclic tests, shows that the maximum strengths in cyclic curves relatively have the same trend with strengths in monotonic curve in general. However, there is a considerable degradation in the strength of cyclic response after a half target displacement (about 10 mm). On average, this strength degradation is about 18.9% for this specimen. In terms of the endured cycles (Nc), the specimen sustained 22 complete loading cycles.

Close to the displacement axis, some horizontal small response is visible in all of the loops, which is due to the gaps devised for easy mounting of the bars. Similar to the results of monotonic test, the yielding points occurred at small displacements, and there was a smooth transition between elastic and inelastic behaviour. Interestingly, it is seen that the specimen exhibits an abrupt increase in stiffness and strength in last steps during large deformation, near to each target displacements. This phenomenon is due to a shift of the dissipating mechanism from flexure to tension in the BFDs.

From Step 5 onwards, some increasing degradations are noticeable in the strength and stiffness of the specimen at the second cycles of steps. On average, this strength degradation is equal to 13% for the six last steps of this specimen. This phenomenon occurs because of low-cycle fatigue life of the applied bars in the device and it can be alleviated by choosing smaller maximum BFD displacements to restrain the amount of degradation in order to satisfy requirements in standards. For this reason, the displacement domain of the BFD is a key parameter in the design of device and it should be wisely chosen in which the BFD dissipates highest possible earthquake energy along with acceptable degradations in both strength and stiffness of the bars.

The key parameters obtained from the force-displacement hysteresis of all specimens, such as the maximum strengths (P_{max} , P_{min}) with corresponding target displacements (D_{max} , D_{min}) in both directions (upward and downward), and the number of sustained cycles (N_c) along with the ratio of target displacement to the bar length (D/L), are listed in Table 6. The Bauschinger effect is noticeable, and on average, the downward strengths are 12.5% higher than the upward strengths. Due to the combined dissipating mechanism, the maximum strengths of the BFDs are on an average 6.30 times higher than the yield strength of the

device, P_y . All of the specimens failed after 20 cycles on average. Considering the relation of the (D/L) ratio with the force-displacement behaviour of the specimens, it is concluded that a smaller ratio gives better hysteretic behaviour of the BFD, with less degradation of the strength and stiffness in the last cycles. Therefore, being on the safe side in the primary design of the BFD, assigning less than 13% to the (D/L) ratio is recommended, to have a robust and stable response and to guarantee more than 20 sustained cycles with less degradation in strength and stiffness. This can be a useful estimation for preliminary design of the device. Moreover, it should be noted that most of the calculated parameters here are dependent on the displacement history, and can be slightly changed with a different loading history.

3.4.3. Equivalent stiffness and damping ratios

One of the most important properties of metallic dampers is an energy dissipation capability that is not dependent on the rate of loading. To have an indication of this capability in order to evaluate and compare metallic dampers, the parameter of the equivalent viscous damping ratio was defined and it has the following relationship [21]:

$$\xi_{eq} = \frac{1}{4\pi} \frac{E_D}{E_S} = \frac{1}{2\pi} \frac{E_D}{K_{eff} D^2} \quad (1)$$

where E_D is the dissipated energy in each cycle of hysteresis equal to the enclosed area of a complete cycle. E_S is the strain energy stored in an elastic spring with an equivalent stiffness K_{eff} and displacement D , whose equation is $\frac{1}{2} K_{eff} D^2$. K_{eff} is the equivalent stiffness, which can be calculated by the maximum strengths and displacements in both directions as in the formula below;

$$K_{eff} = \frac{|P_{max}| - |P_{min}|}{|D_{max}| - |D_{min}|} \quad (2)$$

It should be noted that this damping ratio is a property of the device itself and it differs from the damping ratio of a real structure equipped with the device. A total of 10 last complete cycles of each test result was selected to calculate the equivalent stiffness and the damping ratio of the BFDs. The lower cycles were not used in this calculation because they do not make a considerable contribution to the energy dissipation. The average of the stiffness and damping ratio for the ten last cycles of each BFD is calculated and listed in Table 6. The plots of the equivalent stiffness versus damping ratio for the last five loading steps of six devices with different numbers of bars are shown in Fig. 12. In this figure, each point shows a possible stiffness and damping ratio of the related BFD at the corresponding hysteresis cycle. Remarkably, devices with bars of the same length, but different diameters behave in relatively similar fashions. It can be observed that the damping ratio of the proposed device relates almost inversely to the effective stiffness. In general, the BFD can furnish a damping ratio and effective stiffness in the range of 35–65% and 0.5–6 kN/mm, respectively. It can be concluded that the BFD is capable of dissipating the seismic energy as well as the other available metallic dampers, and is even more advantageous in being simple and economical.

3.4.4. Energy dissipation

The cumulative energy dissipation versus cumulative displacement of all 18 BFDs under cyclic tests is plotted in Fig. 13. Each specimen dissipates energy relatively linearly with the increase of the displacements; there are smaller amounts in the elastic zone and a considerable volume in the inelastic zone. According to the specimens behaviour, the rate of energy dissipation rises up when adding bars, increasing the bar diameter and decreasing the bar length in the BFDs. Overall, the plotted curves show that BFDs can absorb a considerable amount of input energy relative to their low weight, with a cumulative displacement over 600 mm. For example, the three bars with a diameter of 14 mm and total weight of 1 kg in specimen 3Bar14-188 dissipated about 10.5 kJ energy under cyclic loading with 700 mm cumulative displacement.

Table 6
Important results of the cyclic tests and key calculated parameters.

Specimens	P (kN)		D (mm)		Nc	D/L	K_{eff}^{avg} (kN/mm)	Cum. Energy (J)	ξ_{eq}^{avg}
	Max	Min	Max	Min					
1Bar10-158	15.21	-10.34	26	-26	21	0.16	0.58	1382	0.46
2Bar10-158	29.40	-20.77	26	-26	21	0.16	1.18	2810.2	0.46
3Bar10-158	40.40	-30.73	26	-26	21	0.16	1.69	4154.5	0.46
1Bar10-188	14.94	-10.25	30.1	-30.1	19	0.16	0.43	1245.3	0.55
2Bar10-188	29.15	-25.46	30.1	-30.1	20	0.16	0.85	2979.8	0.51
3Bar10-188	40.64	-31.51	30.1	-30.1	20	0.16	1.26	4477.7	0.49
1Bar12-158	20.34	-13.21	20	-20	20	0.13	1.34	2789.3	0.57
2Bar12-158	35.63	-26.08	20	-20	20	0.13	2.61	5586.2	0.57
3Bar12-158	49.91	-38.69	20	-20	20	0.13	3.86	7499.5	0.58
1Bar12-188	19.89	-19.09	30.1	-30.1	19	0.16	0.84	2512.4	0.56
2Bar12-188	33.64	-31.66	26.2	-26.2	20	0.14	1.46	5767.7	0.55
3Bar12-188	48.93	-47.56	26.2	-26.2	20	0.14	2.16	7858.3	0.55
1Bar14-158	20.51	-18.75	20	-20	20	0.13	2.03	3941.1	0.57
2Bar14-158	41.38	-36.96	20	-20	20	0.13	3.75	8115.35	0.57
3Bar14-158	60.67	-54.41	20	-20	20	0.13	5.69	9008.2	0.57
1Bar14-188	22.46	-20.05	26.2	-26.2	20	0.14	1.12	3780.1	0.58
2Bar14-188	44.80	-41.77	26.2	-26.2	20	0.14	2.14	7368.9	0.58
3Bar14-188	66.62	-61.78	26.2	-26.2	20	0.14	3.20	10843.6	0.6

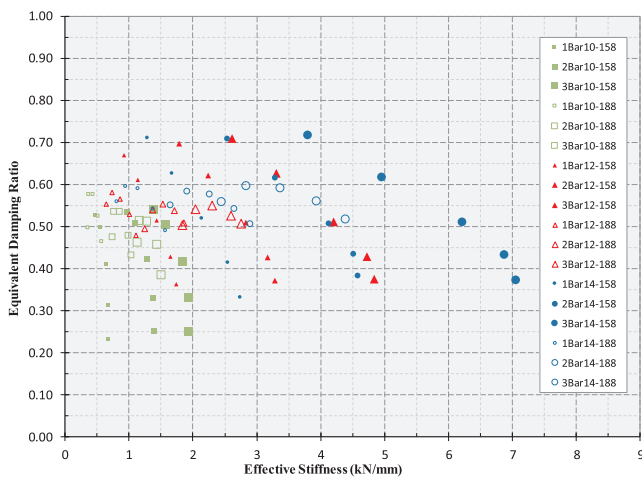


Fig. 12. Equivalent damping ratio vs. effective stiffness of specimens.

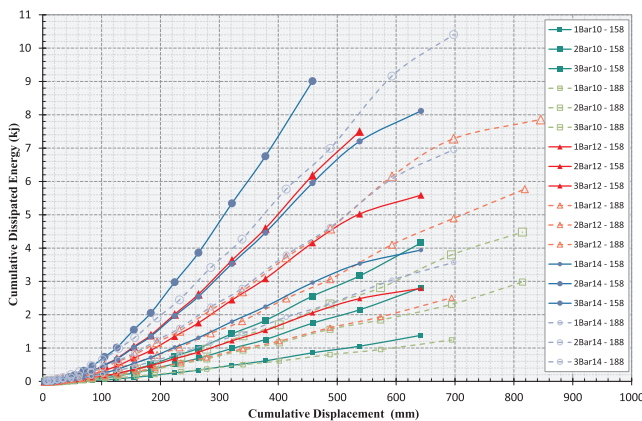


Fig. 13. Cumulative dissipated energy vs. cumulative displacements of the specimens.

3.4.5. Design chart for the BFD

Using the experimental results, a parametric study was carried out to assess the effects of variations in the number, length and diameter of the bars on the behaviour of the BFD. Based on the obtained results of the study, the four below equations (Eqs. (3)–(6)) are recommended for calculation of the key structural properties of a BFD with one bar. These

properties are the yielding strength P_y (N), yielding displacements D_y (mm), elastic stiffness K_0 (N/mm) and ultimate strength P_u (N), which can be determined by the length (L) (mm) and radius (R) (mm) of the bar. The errors of the suggested formulas are all below 10%. To continue, the ultimate strength equation (Eq. (6)) was used to provide a design chart for the BFD as shown in Fig. 14, based on the three main parameters of the bar, namely the length, diameter and strength. Having the buckling capacity of a diagonal brace and assuming the ultimate displacement and the number of bars for the BFD, the preliminary design of the BFD can be easily carried out by choosing the proper length and diameter for the bar through the proposed design chart.

$$P_y = 3410 \frac{R^3}{L} - 335 \tag{3}$$

$$D_y = .0004 \frac{L^2}{R} + 1.30 \tag{4}$$

$$K_0 = 3441 \frac{R^4}{L^3} + 182 \tag{5}$$

$$P_u = 6722 \frac{R^3}{L} + 7981 \tag{6}$$

The BFD can be added in various methods to steel/concrete moment resisting frames for the purpose of seismic retrofitting such as knee braces individually or through braces equipped with the BFD. To improve the seismic performance of a frame, for instance, a steel moment-resisting frame with two columns ($L = 300$ cm) and one beam

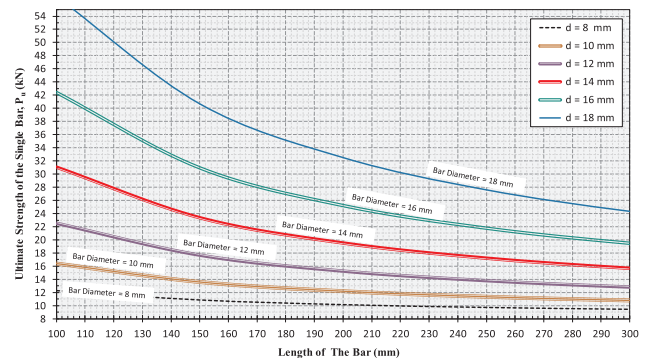


Fig. 14. Design curves for the BFD based on strength, length and diameter of a single bar.

(L = 500 cm) can be equipped with one BFD through one diagonal brace (L = 580 cm) with buckling capacity of 200 kN. Assuming 1% for allowable story drift ratio, the lateral displacement would be limited to 30 mm for the frame. The component of this allowable story drift ratio can be determined in the brace direction by geometric relationships, and is equal to 35 mm. The maximum displacement of the BFD must be taken equal to or smaller than this amount; say 35 mm equivalent to story drift ratio of 1%. Based on the conclusion and recommendation in Section 3.4.2, the bar length can be easily calculated by the obtained relation $(L = 35 \times 1/13\% = 269.2 \text{ mm})$. The equipped brace performs properly when the BFD have a strength equal to or less than the buckling strength of the brace, so the maximum strength of the BFD is taken equal to 200 kN. If the BFD has 10 bars, the strength of each bar should thus be 20 kN $(200/10 = 20 \text{ kN})$. Now, having the length and ultimate strength, 270 mm and 20 kN respectively, the diameter of the bars for the BFD can be selected as 16 mm from the proposed design chart in Fig. 14. Therefore, it is expected that the retrofitted frame with the BFD (10Bar16-270) not only has a better seismic performance under earthquake loads, but also protects the main elements of the frame from failure by sacrificing 10 bars as fuses in the BFD.

3.4.6. Bilinear model for the BFD

A simplified bilinear spring model can be defined for the BFD in order to use it as a metallic yielding damper in any structural analysis software. For this purpose, the maximum force-displacement experimental results of six different devices with one bar are selected and then four lines are approximated for the behaviour of each device, representing the bilinear model. Generally, the response of the BFD can be categorized in three distinguished zones; including elastic, first plastic, and second plastic. Since, the elastic part has a small portion in the response curve, and for simplicity as well, the two initial zones were presented in one line at the proposed model. Therefore, the straight-line interpolations were completed in two phases based on obtained envelopes from the test results; including both first and second zones together, and the third zone individually. For devices with any number of bars, the model can be easily calibrated by increasing the maximum loads linearly concerning the number of bars, while the corresponding displacements remain constant. Fig. 15 shows the proper selected points from experimental results used for the fitting, and the proposed bilinear models for the six BFDs (1Bar10/12/14-158/188) with one bar. The corresponding story drift ratios were also provided in the figures for the six devices, when they were applied in a frame with columns length of 300 cm and an equipped diagonal brace with angle of 25° from the horizontal.

4. Finite element model

The capability of being numerically modelled for a new proposed damper can be considered as a significant feature of the device. For this

purpose, a nonlinear finite element (FE) analysis was performed with the general program of FE analysis, ANSYS (Workbench) [22], to simulate and evaluate the BFD behaviour. All the geometry parts of the outer part, inner parts and the bars were developed in the software, except the channels in the inner part, which do not have a considerable influence on the hysteretic behaviour of the device. Having two perpendicular symmetry planes in the BFD, its quarter was modelled to reduce the mesh numbers and the cost of computation, as shown in Fig. 16(a). The model was meshed with 3D-stress 8-node nonlinear solid elements. All connections of the bars with the inner and outer parts were defined as frictionless because of the small contact area and easy run. However, a bonded contact was assigned to the connections between bars and nuts. Both geometric and material properties were considered as nonlinear in all analyses. The material properties and true strain-stress were exactly defined based on the results obtained from the coupon tests as presented in Table 2. Appropriate supports and boundary conditions were allocated to the BFD and the cyclic load was applied to the model through the middle plate of the inner part in the form of displacement, as the same load protocol used in the experimental tests.

The deformation contour of specimen 3Bar14-188 under a load displacement of 26.2 mm was calculated and shown in Fig. 16(b). As can be seen, the bars deformed under applied displacement through the middle plate of the inner part while the outer part had zero deformation. The equivalent Von-Mises stress and normal elastic strain in the x-direction are also shown in Fig. 16(c) and (d) respectively, for the same specimen under the same conditions. These two contours show clearly that the plastic stress and strain take place in three particular areas of each bar, and are not concentrated in one small area. This property can be considered as an advantage for the BFD in terms of material efficiency on the energy dissipation.

Fig. 17(a) and (b) illustrate the obtained force-displacement hysteresis from FE analyses and experimental results for the two specimens 3Bar12-188 and 3Bar14-188, respectively. As can be seen from the figures, there is a good agreement between the experimental and numerical results in terms of the hysteretic behaviour. However, there are some minor differences in the strength and stiffness of the two related curves at the large displacement. Both kinematic and isotropic hardening rules were tried in the FE analysis and the latter gave a better correspondence to the experimental results. The results attained in the FE analysis show that the BFD has the advantage of being easily modelled in a numerical analysis to simulate the device for further study or use in various applications.

5. Limitations on application of the BFD

The main function of the BFD is to reduce the inelastic energy dissipation demand on frame elements of a structure, and it can be accounted as a damping system in structures. In the codes, e.g. ASCE 7-10

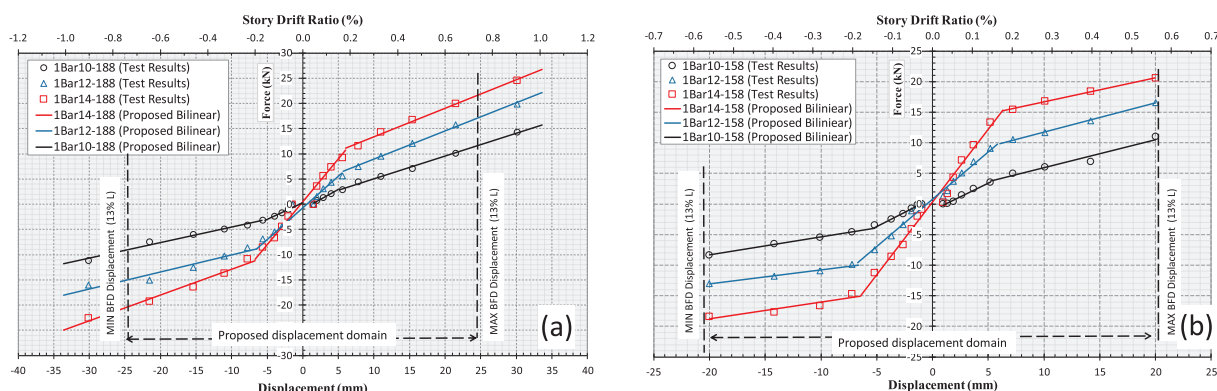


Fig. 15. Proposed bilinear models for six BFDs; (a) 1BFD10/12/14-188, (b) 1BFD10/12/14-158.

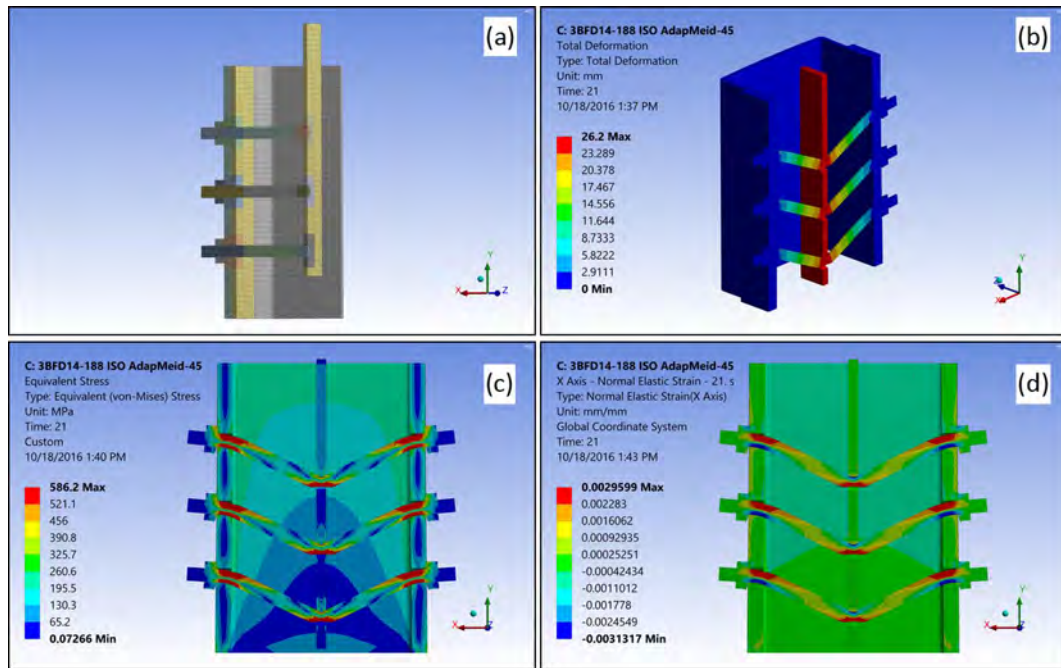


Fig. 16. Finite elements model and analysis results: (a) Mesh of BFD's quarter, (b) deformation contour, (c) Equivalent stress contour (d) Normal Elastic Strain in x-direction.

[23], the damping systems are not permitted to be used alone as a lateral resisting system. A seismic force-resisting system is required in conjunction with the damping system to establish the lateral resisting system of a structure. This force resisting system relative to the damping system sustains a considerable amount of seismic base shear of a structure. Hence, a brace equipped with the BFD cannot be independently considered as a lateral-resisting system of a structure, and it is essential to be utilized with a seismic force-resisting system. The BFD can be adopted with various seismic force-resisting systems in structures, such as moment-resisting frames and braced frames.

It is necessary that damping devices subject to failure by low-cycle fatigue resist wind forces without inelastic cycling [23]. For this reason, a damping system with the BFD is not suitable for high-rise structures which the wind effects are dominant. In buildings that the seismic base shear is significantly greater than the wind induced base shear, it is expected both the BFD and seismic force-resisting system together are able to sustain the wind loads elastically. In this case, therefore, the proposed damper can satisfy the requirement of provision in the standard. Regarding gravity loads, it should be noted that bearing this kind of loads by the proposed device can be detrimental for its performance. Thus, placing the BFD in a suitable location of a system in which it is subjected to the lowest gravity loads, can benefit the performance of the damper to a great extent.

The requirements of story-drift ratio in standards can be easily met in design of the BFD. The code limits are transformable on the brace orientation to correlate with the maximum BFD displacement. For this purpose, the story-drift ratio should be divided by the cosine of angle between the BFD (or the brace) orientation and the horizontal. Assuming a range from 25° to 45° for a diagonal-brace angle in residential buildings, 39 mm for the maximum displacement of BFD with bar length of 300 mm ($300 \text{ mm} \times 0.13 = 39 \text{ mm}$), the studied BFD can accommodate the drift ratio up to 1% determined by the geometric relationships. This margin can be enhanced by increasing both the bar length of BFD and the maximum BFD displacement in where it is feasible.

According to the ASCE 7-10, low-cycle large-displacement degradation should be considered in the design of damping devices due to seismic loads [23]. As an alternative for the seismic load, FEMA461 offers a specific load-protocol in the form of quasi-static cyclic testing, which was used in this study [20]. It is worth noting that, this load-protocol was derived based on 20 different ground motions through investigations. As stated earlier, all the BFDs sustained at least 20 loading cycles in the response of cyclic tests. The average of force degradations at target displacements of the last six steps was about 10.6% in that 20 endured cycles for all 18 specimens. Even though this amount of degradation can satisfy the requirements of device adequacy in the

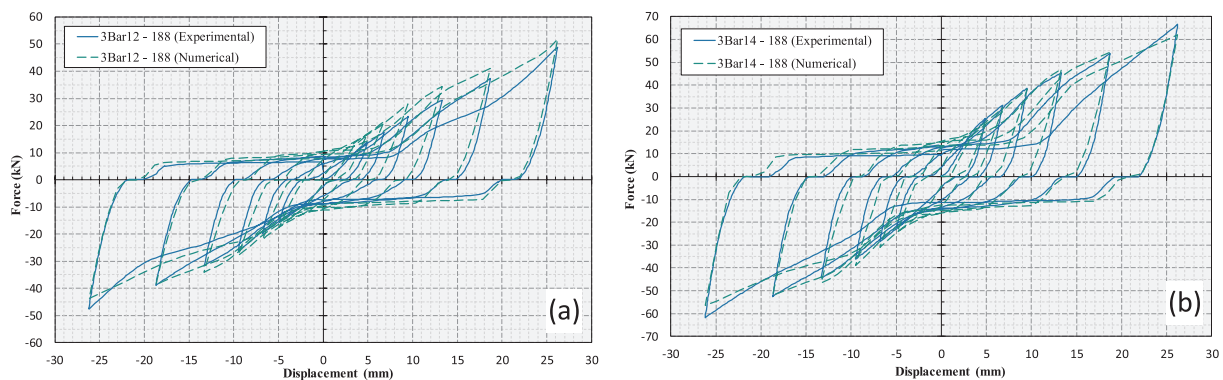


Fig. 17. Comparison of experimental and numerical hysteresis: (a) 3Bar12-188, (b) 3Bar14-188.

standard, it is difficult to claim that whether or not the obtained 20 cycles are enough to avoid the low-cycle fatigue fracture of fuses during an earthquake. Hence, it seems necessary to verify the performance of fuses by further investigations as shake table testing of a frame equipped with the BFD subject to different ground motions. To improve the fatigue life of the fuses in the proposed device, it is expected that using some other materials, e.g. low-yield steel, cast steel, and shape memory alloy can promote the performance of the BFD.

Among several possible locations for installation of the BFD in a frame, the simple way is to add the device by two rigid connectors to two opposite corners of a frame, similar to the configuration of diagonal braces. Since these parts only transmit the axial load to the device, the subjected loads to the device would be axial forces. For this reason, only axial loads to the BFD were considered in this experimental study. In those cases that the BFD is installed in different locations or subjected to loads other than the described ones, the presented results might not be valid, and more investigations would be needed for that specific condition.

6. BFD and other metallic dampers

To evaluate the weak and strong points of the BFD, a comparative study was conducted among the available well-known metallic dampers using important parameters which are presented in Table 7. The results of some other comparison work were also used in this assessment study [16,24]. All the data collected here is based on the experimental results presented in the relevant papers. In some cases, the parameters were estimated or calculated. Ten metallic yielding dampers were selected for comparison with the BFD: Pipe Damper (PD) [14], Dual-Pipe Damper (DPD) [15], Infilled-Pipe Damper (IPD) [16], Triangular-plate Added Damping and Stiffness (TADAS) [10], Slit-Damper (SD) [11], Shear Panel Damper (SPD) [13], Honeycomb Damper (HD) [25], Cast Steel Yielding Brace (CSYB) [12], Double Function Metallic Damper X-Shaped (DFDMX) [26], and Box-Shaped Slit Damper (BSSD) [27].

Comparison of the key parameters of the BFD with the other

dampers shows that the recommended device is able to compete well with other available metallic-yielding dampers. In some parameters, the BFD has advantages over the other dampers. Having the lowest mass of the bar element causes the BFD to have the highest maximum force to mass ratio among the dampers, which proves the material efficiency of this device. This ratio shows the strength of the energy absorber element for the unit mass of the used material. Also, the BFD got high marks for being economical, the replaceability and installation of the damper, as seen in Table 7. Overall, it is seen that the BFD can be one of the top devices in the ranking list of metallic dampers.

7. Summery and conclusions

In this paper a new passive earthquake damper, the Bar-Fuse Damper (BFD), was presented and evaluated both experimentally and numerically. The performance of the BFD was assessed with more than 30 monotonic and cyclic experiments, and the applied bars successfully performed their function as energy absorbers and fuses in all the specimens. The proposed device showed appropriate ductility, energy absorption and stable hysteretic behaviour under cyclic loads without any sudden strength and stiffness degradation. The performance of the BFD depends highly on the nut arrangements of the bars. The simplest design, two nuts on the both ends of the threaded bar, gave a reliable behaviour to the proposed device, as well as the possibility of convenient placing and replacing the bars when they were failed. This proper replacement capability can be considered as a key feature of the proposed device over to other available metallic dampers.

All the applied steel bars as fuses in the proposed device sustained more than 20 loading cycles with cumulative displacement of over 600 mm in the quasi-static cyclic tests along with an average on strength degradation about 10.6% at target displacements of the last six steps. This achieved by taking the maximum BFD displacement equal to 13% of the bar length. In general, the BFD was able to furnish an equivalent viscous damping ratio in the range of 35–65%. Due to the combined flexural-tensile mechanism of the device, the ultimate

Table 7
Key parameters of several metallic yielding dampers and the BFD.

Parameters	Yielding metallic dampers										
	PD ^a	DPD ^b	IPD ^c	TADAS ^d	SD ^e	SPD ^f	HD ^g	CSYB ^h	DFDMX ⁱ	BSSD ^j	BFD ^k
Yield displacement (mm)	2.5–4	1.6–2.1	0.80–3.20	1.1–5.8	0.3–0.49	0.7–5.2	NA	4.5	1.5	0.51	1.9–3.17
Initial stiffness (kN/mm)	0.5–4.5	7.5	17–39.2	14–72	6.7–14.6	1.3–44.9	NA	8.9	1.80–3.80	31.8	0.45–5.80
Equivalent damping ratio	0.4	0.45	0.36	0.46	0.30–0.50	0.10–0.30	0.45	0.41	0.46	0.34	0.30–0.60
Total dissipated energy (kJ)	NA [*]	49.2	242	NA	6.9–10.3	5.8–6.51	NA	NA	NA	NA	1.2–3.9 ^{**}
Cumulative displacement (mm)	NA	1130	2100	NA	500	325–400	NA	1888	353.3	NA	458–845
Ductility	20	20	27.8	22	29–40	8.5	6	8.7	17.1	60	17.1
Mass (kg)	0.7–1.0	2.1–6.6	49.7	95.8	2.2	1.6	10.4	NA	1.3	17	0.17–0.34
Height (mm)	114–140	110–140	220	304	162	100–120	135	NA	180	80	158–188
Deformation capacity Ratio	0.44	0.36	0.32	0.29	0.12	0.14–0.20	0.29	NA	0.07	0.37	0.21
Max. force-to-mass ratio (kN/kg)	11.4	19.9	5.4	12.8	16.2	22.6	17.9	NA	22	10.59	59–89.5
Cost of Damper fabrication	Low	Low	High	High	Medium	Medium	Medium	High	Medium	Medium	Medium
Installation of damper	Easy	Easy	Easy	Difficult	Easy	Easy	Easy	Difficult	Easy	Easy	Easy
Replaceability ^l	Medium	Medium	Difficult	Difficult	Medium	Medium	Medium	Difficult	Medium	Medium	Easy

^a Pipe damper.
^b Dual-pipe damper.
^c Infilled-pipe damper.
^d Triangular-plate added damping and stiffness.
^e Slit damper.
^f Shear-panel damper.
^g Honeycomb damper.
^h Cast steel yielding brace.
ⁱ Double-function metallic damper X-shape.
^j box-shaped slit damper.
^k Bar-Fuse Damper.
^l Replaceability of energy absorber element or damper itself.
^{*} Not Available.
^{**} Dissipated energy for a single bar.

strength of the BFD was greater than the corresponding yield strength by a factor of more than 6, which enhances the capacity of energy dissipation. On average, the unit weight of the employed steel bars sustained 75 kN force and dissipated 10.5 kJ input energy.

The comparative study showed that the BFD can be ranked in one of the top places on the list of metallic-yielding dampers by three dominant factors: economical, low-weight and replaceability of the bars as energy absorber components. While the proposed device shows promising results in this feasibility study, it is believed that some further experimental researches as shake table testings on a frame equipped with the BFD are essential before practical application of the device.

Appendix A. Supplementary material

Supplementary data associated with this article can be found, in the online version, at <http://dx.doi.org/10.1016/j.engstruct.2017.12.049>.

References

- [1] Soong TT, Spencer BF. Supplemental energy dissipation: state-of-the-art and state-of-the-practice. *Eng Struct* 2002;24:243–59. [http://dx.doi.org/10.1016/S0141-0296\(01\)00092-X](http://dx.doi.org/10.1016/S0141-0296(01)00092-X).
- [2] Fisco NR, Adeli H. Smart structures: Part I – active and semi-active control. *Sci Iran* 2011;18:275–84. <http://dx.doi.org/10.1016/j.scient.2011.05.034>.
- [3] Symans MD, Asce AM, Charney FA, Asce F, Whittaker AS, Asce M, et al. Energy dissipation systems for seismic applications: current practice and recent developments. *J Struct Eng* 2008;134:3–21. [http://dx.doi.org/10.1061/\(ASCE\)0733-9445\(2008\)134:1\(3\)](http://dx.doi.org/10.1061/(ASCE)0733-9445(2008)134:1(3)).
- [4] Parulekar YM, Reddy GR. Passive response control systems for seismic response reduction: a state-of-the-art review. *Int J Struct Stab Dyn* 2009;9:151–77.
- [5] Muto K. Earthquake resistant design of 36-storied Kasumigaseki building. *Proc 4th World Conf Earthq Eng*, vol. 3. 1969. p. 16–33.
- [6] Guerrero J. Bandas amortiguadoras para muros de partición (damping strips for partition walls). In: *Memorias del Prim. Congr. Nac. Ing. Sísmica*, Spanish; 1965. p. 75–85.
- [7] Kelly JM, Skinner RI, Heine AJ. Mechanisms of energy absorption in special devices for use in earthquake resistant structures. *Bull NZ Soc Earthq Eng* 1972;5:63–88.
- [8] Skinner RI, Kelly JM, Heine AJ. Hysteretic dampers for earthquake-resistant structures. *Earthq Eng Struct Dyn* 1975;3:287–96. <http://dx.doi.org/10.1002/eqe.4290030307>.
- [9] Wada A, Huang Y-H, Iwata M. Passive damping technology for buildings in Japan. *Prog Struct Eng Mater* 2000;2:335–50. [http://dx.doi.org/10.1002/1528-2716\(200007/09\)2:3<335::AID-PSE40>3.0.CO;2-A](http://dx.doi.org/10.1002/1528-2716(200007/09)2:3<335::AID-PSE40>3.0.CO;2-A).
- [10] Tsai K, Chen Huan-Wei, Hong Ching-Ping, Su Yung-Feng. Design of steel triangular plate energy absorbers for seismic-resistant construction. *Earthq Spectra* 1993;9:505–28. <http://dx.doi.org/10.1193/1.1585727>.
- [11] Chan RWK, Albermani F. Experimental study of steel slit damper for passive energy dissipation. *Eng Struct* 2008;30:1058–66. <http://dx.doi.org/10.1016/j.engstruct.2007.07.005>.
- [12] Gray MG, Christopoulos C, Packer JA. Cast steel yielding fuse for concentrically braced frames. 9th US Natl. 10th Can. Conf. Earthq. vol. 6. 2010. p. 4235–44. Toronto, Ontario, Canada.
- [13] Chan RWK, Albermani F, Kitipornchai S. Experimental study of perforated yielding shear panel device for passive energy dissipation. *J Constr Steel Res* 2009;65:260–8. <http://dx.doi.org/10.1016/j.jcsr.2013.08.013>.
- [14] Maleki S, Bagheri S. Pipe damper, Part I: experimental and analytical study. *J Constr Steel Res* 2010;66:1088–95. <http://dx.doi.org/10.1016/j.jcsr.2010.03.010>.
- [15] Maleki S, Mahjoubi S. Dual-pipe damper. *J Constr Steel Res* 2013;85:81–91. <http://dx.doi.org/10.1016/j.jcsr.2013.03.004>.
- [16] Maleki S, Mahjoubi S. Infilled-pipe damper. *J Constr Steel Res* 2014;98:45–58. <http://dx.doi.org/10.1016/j.jcsr.2014.02.015>.
- [17] Rezaei M, Prion H, Tremblay R. Seismic performance of brace fuse elements for concentrically steel braced frames. In: *STESSA 2000 Conf*, Montreal, Canada; 2000. p. 39–46.
- [18] Tremblay R, et al. Overview of ductile seismic brace fuse systems in Canada. In: *EuroSteel 2011*, Budapest, Hungary; 2011. p. 939–44.
- [19] ASTM Int. ASTM A370. Test methods for tension testing of metallic materials 1. *Astm* 2009;1:1–27. <http://dx.doi.org/10.1520/E0008>.
- [20] FEMA 461. Federal Emergency Management Agency. testing protocols for determining the seismic performance characteristics of structural and nonstructural. Washington, DC; 2007.
- [21] Chopra A. *Dynamics of structures, theory and applications to earthquake engineering*. 4th ed. Prentice Hall; 2012.
- [22] ANSYS Inc., Workbench user's guide. ANSYS Man 2013;15317:724–746.
- [23] ASCE/SEI 7-10. American Society of Civil Engineers. Minimum design loads for buildings and other structures, Reston, Virginia; 2007.
- [24] Aghlara R, Md. Tahir M, Adnan A. Comparative study of eight metallic yielding dampers. *J Teknol* 2015;77:119–25. <http://dx.doi.org/10.11113/jt.v77.6408>.
- [25] Kobori T, Miura Y. Development and application of hysteresis steel dampers. In: *Earthq. Eng. Tenth World Conf.*, Balkema, Rotterdam; 1992. p. 2341–2346.
- [26] Li G, Li H. Earthquake-resistant design of RC frame with “Dual Functions” metallic dampers. In: *14th World Conf. Earthq. Eng.*, Beijing, China; 2008. p. 43–53. <http://dx.doi.org/10.1115/PVP2007-26450>.
- [27] Lee J, Kim J. Development of box-shaped steel slit dampers for seismic retrofit of building structures. *Eng Struct* 2017;150:934–46. <http://dx.doi.org/10.1016/j.engstruct.2017.07.082>.